ACS NANO

www.acsnano.org

ARTICLE

Rotation of Ethoxy and Ethyl Moieties on a Molecular Platform on Au(111)

Torben Jasper-Toennies,* Manuel Gruber,* Sven Johannsen, Thomas Frederiksen, Aran Garcia-Lekue, Torben Jäkel, Fynn Roehricht, Rainer Herges, and Richard Berndt

Cite This: *ACS Nano* 2020, 14, 3907−3916

Read Online

ACCESS | Metrics & More | Article Recommendations | Supporting Information

ABSTRACT: **Molecular rotors have attracted considerable interest for their prospects in nanotechnology. However, their adsorption on supporting substrates, where they may be addressed individually, usually modifies their properties. Here, we investigate the switching of two closely related three-state rotors mounted on platforms on Au(111) using low-temperature scanning tunneling microscopy and density functional theory calculations. Being physisorbed, the platforms retain important gas-phase properties of the rotor. This simplifies a detailed analysis and permits, for instance, the identification of the vibrational modes involved in the rotation process. The symmetry provided by the platform enables active control of the rotation direction through electrostatic interactions with the tip and charged neighboring adsorbates. The present investigation of two model systems may turn out useful for designing platforms that provide directional rotation and for transferring more sophisticated molecular machines from the gas phase to surfaces.**

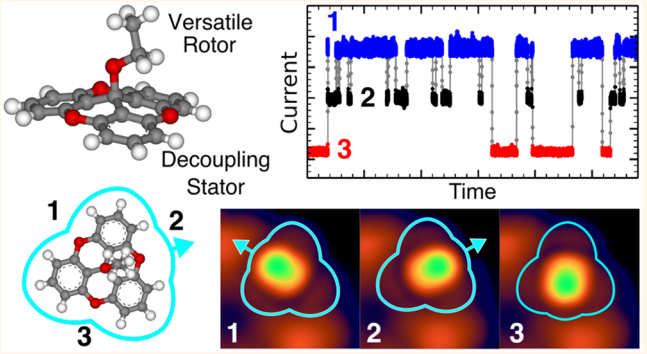

KEYWORDS: *scanning tunneling microscopy, rotor, platform approach, action spectroscopy, directional*

Switches and motors are essential engineering components in our macroscopic world as well as at the molecular level.[1,2] Considerable effort is made to synthesize artificial motors that mimic biological examples or offer prospects in nanotechnology.[3] Rotor molecules deposited on surfaces may be investigated at a submolecular scale using scanning tunneling microscopy (STM).[4,5] The compounds thus studied fall into two classes. Either molecular adsorbates serve as a rotor and the substrate is used as a stator[6−21] or the stator and the rotor are subunits of the same molecule.[22−26] Besides rotors there are also rotary switches that alternate between two rotation angles[27−31] and consequently do not enable studies on the directionality of the motion, which is essential for using a rotor in a motor.[3,4]

The adsorption of molecules on surfaces often modifies their gas-phase properties. While these modifications may be beneficial, *e.g.*, by inducing an asymmetry,[32] which is essential for the directionality of the rotation,[26,33,34] they render predictions of the on-surface properties of a molecule difficult.

Here, we investigate two closely related three-state stepper motors using STM and density functional theory (DFT) calculations. In contrast to previous studies, we employ a rigid and planar molecular platform, namely, trioxatriangulenium (TOTA),[35] as anchor rather than using single atoms, such as sulfur,[23−25] or flexible molecular subunits.[26] The platform serves as stator, separates the rotor from the substrate,[36−38] and provides an electronic decoupling because it binds to Au surfaces *via* physisorption,[37,38] in contrast to most chemically bonded platforms.[39] We show that this approach preserves important gas-phase properties of the molecules, such as the rotational energy barriers and the vibrational modes involved in rotation. Inelastic electron tunneling excites the relevant vibrations, which in turn switch the orientation of the rotors. Although the molecules are achiral, directionality of the rotational steps is induced and controlled through the interaction with the STM tip or neighboring adsorbates. The electronic decoupling provided by the platform effectively increases the switching yield of the rotor and may lead to a longer lifetime of electronic excited states of the rotor, which would be useful to control the rotation by light.[40−42]

Received: January 2, 2020
Accepted: February 19, 2020
Published: February 19, 2020

https://dx.doi.org/10.1021/acsnano.0c00029
ACS Nano 2020, 14, 3907−3916

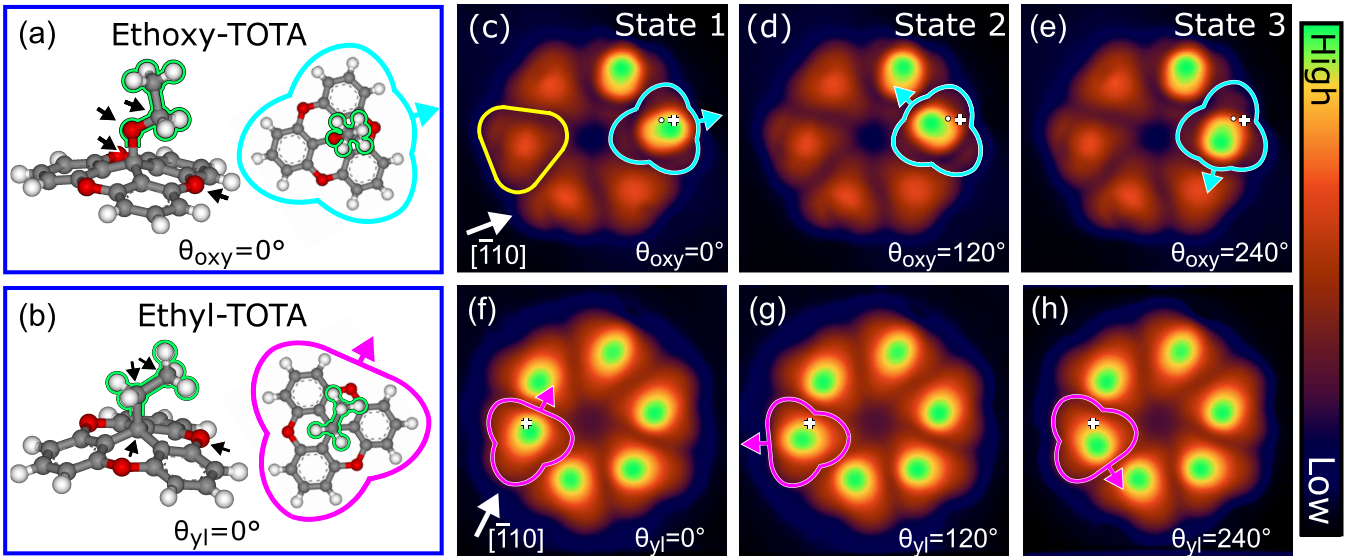

Figure 1. (a, b) Gas-phase molecular structure of ethoxy-trioxatriangulenium (ethoxy-TOTA) and ethyl-TOTA. Gray, red, and white spheres indicate carbon, oxygen, and hydrogen atoms. The torsion angles θ_{oxy} and θ_{yl} of the ethoxy and ethyl moieties (encircled in green) are defined by the four atoms that are highlighted by black arrows in (a) and (b). (c–e) STM topographs showing current-induced switching (image size (3.9 nm)^2, current I = 30 pA, sample voltage V = 100 mV). An ethoxy-TOTA molecule (turquoise border) in a hexagonal cluster of two ethoxy-TOTA and four OH-TOTA molecules (example marked with a yellow border) is switched by injecting current at the position of the white cross. A turquoise-colored arrow shows the orientation of the ethoxy group. Starting from θ_{oxy} = 0 in (c), 120° and 240° are obtained in (d) and (e). (f–h) Analogous data from a cluster comprising six ethyl-TOTA molecules. From (f) to (h) the direction of the CH_2–CH_3 bond of the ethyl moiety within the marked molecule is switched into three configurations with θ_{yl} = 0°, 120°, and 240°. The STM images were processed by merging the raw data with a smoothed and inverted Laplace-filtered image to enhance the contrast. In the raw images the maximum apparent heights of OH-TOTA, ethyl-TOTA, and ethoxy-TOTA molecules are 0.21, 0.26, and 0.31 nm, respectively.

RESULTS AND DISCUSSION

Three-State Rotors. Ethoxy-TOTA and ethyl-TOTA molecules (Figure 1a and b) were designed to serve as three-state rotors with the versatile TOTA platform adsorbed to the substrate as stator and the central moiety as rotor. Although the platform physisorbs, its adsorption energy on a metal surface is close to that of a chemical bond owing to the lateral extension of the molecule, *i.e.*, on the order of 1 eV (100 kJ/mol).[37,38] The ethoxy and ethyl moieties are freestanding and inclined with respect to the metal substrate[37,38] and are located in one of the three mirror planes of the C_{3v} symmetric platform (see topviews in Figure 1a and b). Two hydrogen atoms of the moieties bind *via* a CH···O hydrogen bond to one of the three oxygen atoms of the platform. In addition, ethyl-TOTA has two further CH···O bonds to the remaining two oxygen atoms of the platform. Switching between the three symmetry-equivalent positions corresponds to a rotation of the moiety, *i.e.*, a change of its torsion angle. As the molecules exhibit a C_{3v} symmetry, no directional rotation is expected.

Adsorption Geometry. In two separate experiments, ethoxy-TOTA mixed with OH-TOTA molecules and ethyl-TOTA molecules (Figure 1a and b) were sublimated onto Au(111) at ambient temperature and studied with STM at 4.6 K (see Methods). At low coverages, the intact TOTA molecules self-assemble into clusters composed of six molecules. Single molecules (Figure 1c and f, ethoxy-TOTA: turquoise bordered, OH-TOTA: yellow bordered, ethyl-TOTA: magenta bordered) are imaged as triangular protrusions in accordance with the symmetry of the platform.

The orientation of the moiety of ethoxy-TOTA is discernible by its off-center position and the elliptic shape of the highest areas of the image (green-colored area, Figure 1c). For example, the configuration of the ethoxy-TOTA in Figure 1c (turquoise) is equal to that in the model in Figure 1a. Analogous data from ethyl-TOTA are shown in Figure 1f (magenta).

The three possible orientations of the moieties translate into three torsion angles θ_{oxy} and θ_{yl} that are defined *via* the four atoms marked in Figure 1a and b. STM topographs (Figure 1c and f) reveal that the stable orientations θ_{oxy} (θ_{yl}) of the ethoxy (ethyl) moiety, namely, 0°, 120°, and 240°, are identical to those of the gas-phase molecules. θ_{oxy} = 0° (θ_{yl} = 0°) is defined as the torsion angle for which the mirror plane of the molecule is approximately parallel to the [1̄10] direction of Au(111) (*cf.* Figure 1c and f).

Tunneling-Induced Moiety Rotation. The torsion angle can be changed by injecting current through the molecules at suitable sample voltages and positions. For example, in Figure 1c–e the ethoxy-TOTA molecule (turquoise) was switched from θ_{oxy} = 0° to 120° and then to 240°. Analogous data for ethyl-TOTA (magenta) are displayed in Figure 1f–h. The switching is molecule-selective and does not affect any neighbors as long as mild parameters (V < 400 mV, I < 500 pA) are used.

To efficiently read out the torsion state of a molecule, the STM tip was positioned over it at a specific position indicated by a white cross in Figure 1c–e and f–h. This position breaks the molecular symmetry and leads to characteristic currents (feedback off) or heights (feedback on). It may be noted that this detection scheme has previously been used for, *e.g.*, oxygen molecules on Pt(111)[7] and thioether on Au(111).[8] After moving the tip to such a position, the sample voltage was increased until abrupt changes of the current were observed (feedback off). Figure 2 shows a typical time series of the

https://dx.doi.org/10.1021/acsnano.0c00029
ACS Nano 2020, 14, 3907–3916

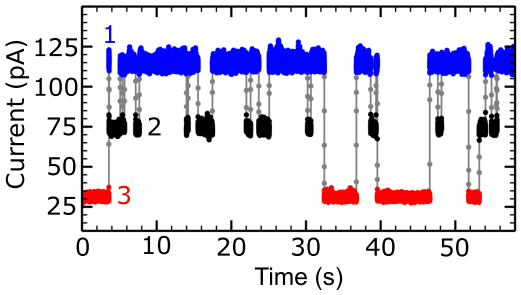

Figure 2. (a) Time series of the tunneling current measured with the tip positioned over an ethoxy-TOTA molecule. The corresponding lateral tip position is indicated by a white cross in Figure 1c–e. A sample voltage V = 185 mV was applied, and the current feedback was opened at a current I = 27 pA. The current levels 1–3 correspond to states 1–3 (cf. Figure 1c–e). Intermediate current values (gray points) are measured because the bandwidth-limited signal from the transimpedance amplifier was oversampled.

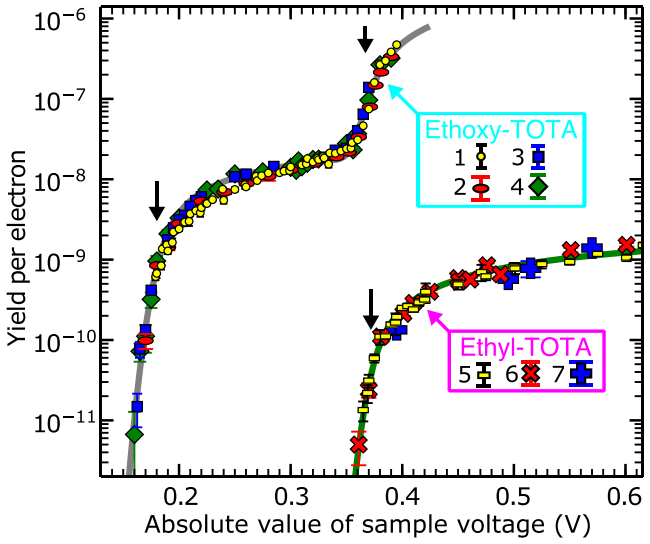

Figure 3. (a) Yield (switching probability per electron) *vs* |*V*| for ethoxy-TOTA (symbols 1–4) and ethyl-TOTA (symbols 5–7). Current was injected into ethoxy-TOTA (ethyl-TOTA) at the position of the white cross in Figure 1c–e (Figure 1f–h). Data sets 2 and 6 were recorded at negative *V*. Bars indicate the standard deviation σ expected from a Poisson process. Fits using eq S1 (gray and green lines) reveal that vibrational modes at energies of 180 ± 2 and 367 ± 2 meV for ethoxy-TOTA and 371 ± 3 meV for ethyl-TOTA (black arrows) are involved in the switching processes. Data sets 3 and 4 were acquired on a molecule adjacent to a six-molecule cluster, *i.e.*, with a single neighbor. The best agreements are obtained with widths of the vibrational density of states (vDOS) $\sigma_G \lesssim$ 10 meV (eq S4).

tunneling current from an ethoxy-TOTA molecule at V = 185 mV. Three distinct levels (1–3) are discernible with average currents of 115 pA, 75 pA (−35%), and 33 pA (−71%) colored in blue, black, and red, respectively. Using additional topographs, we verified that the levels reflect states θ_{oxy} = 0°, 120°, and 240°, respectively. Ethoxy-TOTA and ethyl-TOTA can actually be set to a desired state (0°, 120°, and 240°) by rapidly reducing the sample voltage once the corresponding target current is reached. The switching does not show any sign of fatigue, even after tens of thousands of events.

The switching rate R, defined as the number of detected switching events per time interval, depends crucially on the tunneling current I. At a given voltage and for I < 500 pA, we find $R \propto I^N$ with $N \approx 1$ (not shown). The reaction order of 1 indicates that, while a large fraction of the electrons elastically tunnels without affecting the state of the investigated molecule, the switching is induced by single-electron tunneling. In that respect, the energy transfer from a single tunneling electron is sufficient to change the state of the adsorbate. At smaller tip–molecule distances, *i.e.*, higher currents, mechanical contact may play a role, too.[38] Here, we focus on results obtained at large separations.

Action Spectroscopy. Action spectra, *i.e.*, the switching yields $Y = R/(I/e)$ (e: electron charge) per electron as a function of the sample voltage,[43−45] were measured for both molecules (Figure 3). As the switching rate R is proportional to the current I, the yield Y is approximately constant at fixed V. The action spectra of ethoxy-TOTA and ethyl-TOTA are drastically different (Figure 3). In particular, while the minimal voltage to efficiently switch ethoxy-TOTA ($Y \gtrsim 10^{-11}$) is ∼160 mV, this voltage has to be more than doubled (∼360 mV) for ethyl-TOTA. This difference is rather surprising because the binding of the TOTA stator molecules to Au(111) is virtually identical (see below) and both moieties are attached *via* sp^3 σ bonds (*cf.* Figure 1a and b).

The evolutions of $Y(V)$ in Figure 3 are typical of switching events that are induced by single-electron tunneling *via* vibrational excitation of the molecules.[43,45] For this scenario an analytic expression for $Y(V)$ was derived in ref 44 (see also eqs S1 and S2 in SI) that we used to fit the data (gray and green lines in Figure 3). The fits reveal two vibrational modes at 180 ± 2 and 367 ± 3 meV for ethoxy-TOTA and one mode at 371 ± 1 meV for ethyl-TOTA (see arrows in Figure 3). It should be noted that a similar quality of the fits can be achieved by using several modes whose energies differ by less than ∼10 meV from the aforementioned values. The experimental data consequently do not enable the identification of a *single* vibrational mode. For ethoxy-TOTA, only the onset of the second drastic yield increase at $|V| \gtrsim 360$ mV could be measured because the switching became too rapid to be resolved with our STM at pA currents.

The onsets of abrupt increases are essentially dictated by the energies and the spectral form of the vibrational modes involved in the process (SI, Section I and ref 44). The increases at |*V*| > 200 and <350 mV for ethoxy-TOTA and |*V*| > 390 mV for ethyl-TOTA can be modeled with the expression (SI, Section I)

$$Y(|V|) = K\left(1 - \frac{\hbar\Omega}{|eV|}\right)\theta(|eV| - \hbar\Omega) \quad (1)$$

where K is a dimensionless prefactor, $\hbar\Omega$ the vibrational mode energy, and θ is the step function, which extends the definition of eq 1 to voltages $|eV| < \hbar\omega$. The energies of the tunneling electrons range from 0 to |*eV*|. Assuming a constant density of states, the factor $(1 - \hbar\Omega/|eV|)$ corresponds to the fraction of the current for which the electron energies exceed $\hbar\Omega$; that is, it describes the fraction of tunneling electrons that can excite the vibrational mode.

At first glance, K may seem to be closely related to the probability of vibrational excitation by tunneling electrons, which is typically on the order of 0.01 to 0.1.[46−48] However, to lowest order in the electron-vibration coupling, the inelastic cross section approximately cancels out from K because the competing electron–hole pair creation rate of the vibrational

https://dx.doi.org/10.1021/acsnano.0c00029
ACS Nano 2020, 14, 3907−3916

mode varies in a similar manner (see SI, Section 1 and refs 44, 45). Therefore, the prefactor K is mainly determined by the (anharmonic) decay rate γ_{RC} of the excited vibrational mode into the rotation coordinate. In the case of ethoxy-TOTA $K \approx 3.4 \times 10^{-8}$ is more than 1 order of magnitude larger than for ethyl-TOTA ($\sim 3.2 \times 10^{-9}$). The second rise of the yield for ethoxy-TOTA further increases this ratio to more than 3 orders at ~400 mV. This drastic increase suggests that ethoxy-TOTA transfers energy from the excited vibrational modes to the reaction coordinate more efficiently despite the fact that relevant vibrational mode energies are almost identical (~370 meV). We would like to stress that in the off-resonant regime the prefactor K, and henceforth the yield at a given voltage, is proportional to $1/\Gamma^2$, where Γ is related to the electronic coupling of the adsorbate to the substrate (SI, Section I). Therefore, electronic decoupling, provided for instance by the platform itself or by employing a thin insulating layer, may significantly increase the yield of a rotor.

Vibrational Modes Involved in the Rotation. Ethoxy-TOTA and ethyl-TOTA both physisorb to Au(111) in a typical configuration for functionalized TOTA platforms, namely, on *hcp* or *fcc* sites with an orientation consistent with that revealed by STM topographs (Figure 1c and f).[38,49] To understand the different action spectra in Figure 3, it is sufficient to consider DFT calculations for the isolated molecules (see Methods). The calculated energy barriers for the rotation of the attached moieties are quite different, namely, 140 meV for ethoxy-TOTA and 195 meV for ethyl-TOTA. The geometries of the CH···O bonds between the attached moieties and the platform that fix the orientation are hardly different (calculated H···O distances of 0.29 to 0.30 nm). Moreover, the geometries of the transition states are similar. Therefore, we attribute the higher energy barrier for ethyl-TOTA mainly to the two additional CH···O bonds of the CH_2 unit of the ethyl moiety that is directly attached to the central C atom of the platform (H···O distance of 0.30 nm, Figure 1a and b).

In contrast to the energy barriers for the rotation, the computed vibrational spectra of ethoxy-TOTA and ethyl-TOTA are found to be very similar and reveal a gap between ~200 (C−H bending) and 350 meV (C−H stretch) (Figure 4). The calculated vibrational density of states (vDOS) are consistent with infrared spectra of powder samples (not shown). The rotation is assumed to be due to an overbarrier process (in contrast to tunneling processes) because no switching was observed with voltages lower than the energy barrier of the investigated rotor, even after days of measurements. Therefore, all vibrational modes with an energy lower than 140 meV (dashed turquoise line in Figure 4a) and 195 mV (dashed magenta line in Figure 4a) for respectively ethoxy- and ethyl-TOTA are irrelevant for the rotation.

The fit of the action spectrum of ethyl-TOTA revealed vibrational modes at ~370 meV (Figure 3, right arrow in Figure 4). In this energy range, we find only C−H stretching modes that are located to the moieties (*cf.* Figure 4a). Another set of C−H stretch modes around 390 meV involves the outer H atoms of the platform. The absence of an additional increase of the switching yields above 370 mV leads us to conclude that the platform modes do not efficiently couple to the rotation, despite their large energy. Calculated vibrational modes located on the moiety are displayed in the SI (Section II). Most of modes of the ethyl group with an energy ~370 meV involve significant displacements of the hydrogen atoms, which

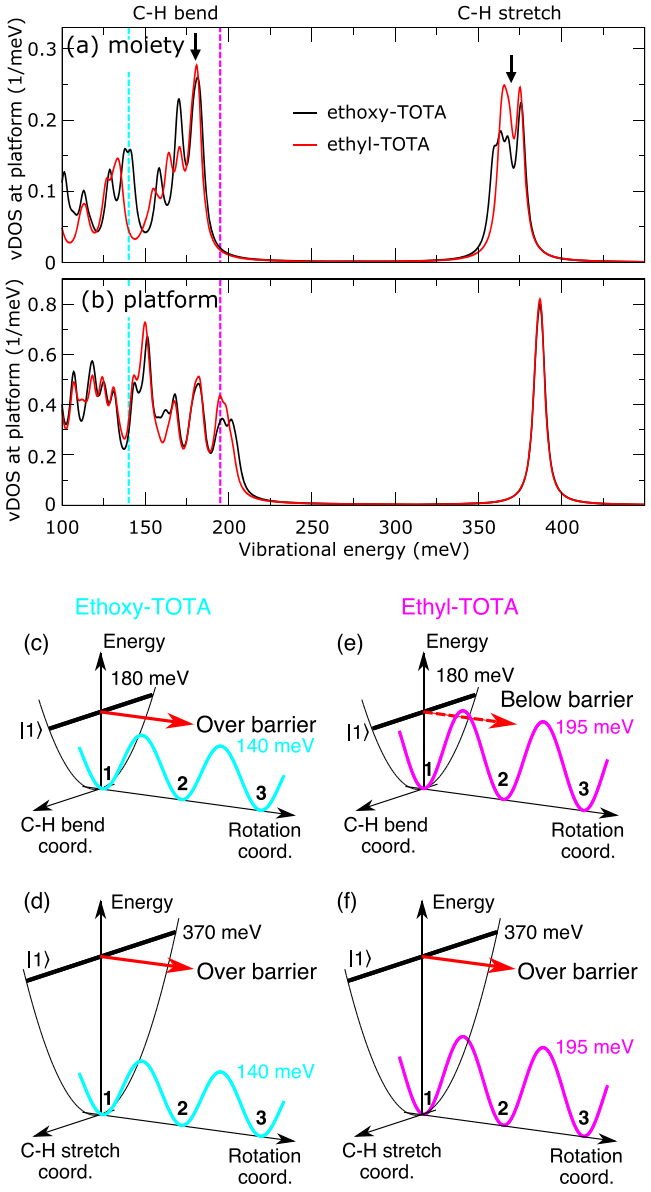

Figure 4. (a) Calculated vibrational density of states (vDOS) projected onto the ethoxy moiety of ethoxy-TOTA (black line) and onto the ethyl group of ethyl-TOTA (red line). The discrete spectra were broadened by 3 meV. Turquoise and purple dashed vertical lines indicate the computed energy barriers for the rotation reaction for ethoxy-TOTA and ethyl-TOTA, respectively. The arrows indicate the vibrational-mode energies extracted from the fits to the data shown in Figure 3. (b) Corresponding vDOS projected onto the TOTA platform for ethoxy-TOTA (black line) and ethyl-TOTA (red line). (c−f) Illustrations of the relevant vibrational modes (C−H stretch and bend) and rotation barriers. The turquoise and purple curves describe idealized rotational energy potentials with energy barriers of respectively 140 and 195 mV. The indexes 1, 2, and 3 represent the three stable orientations of the respective rotors. Along the vibration coordinate, only the relevant C−H bending (c, e) and C−H stretching (d, f) modes of the moieties are shown (180 meV and 370 mV). The solid (dashed) red arrow is a representation of energy transfer from the vibration to the rotation coordinate in an overbarrier (tunneling) process.

mediate hydrogen bonding to the platform. The rotation in ethyl-TOTA is therefore due to one or several C−H stretching vibrational mode(s) located on the moiety, which most likely

https://dx.doi.org/10.1021/acsnano.0c00029
ACS Nano 2020, 14, 3907−3916

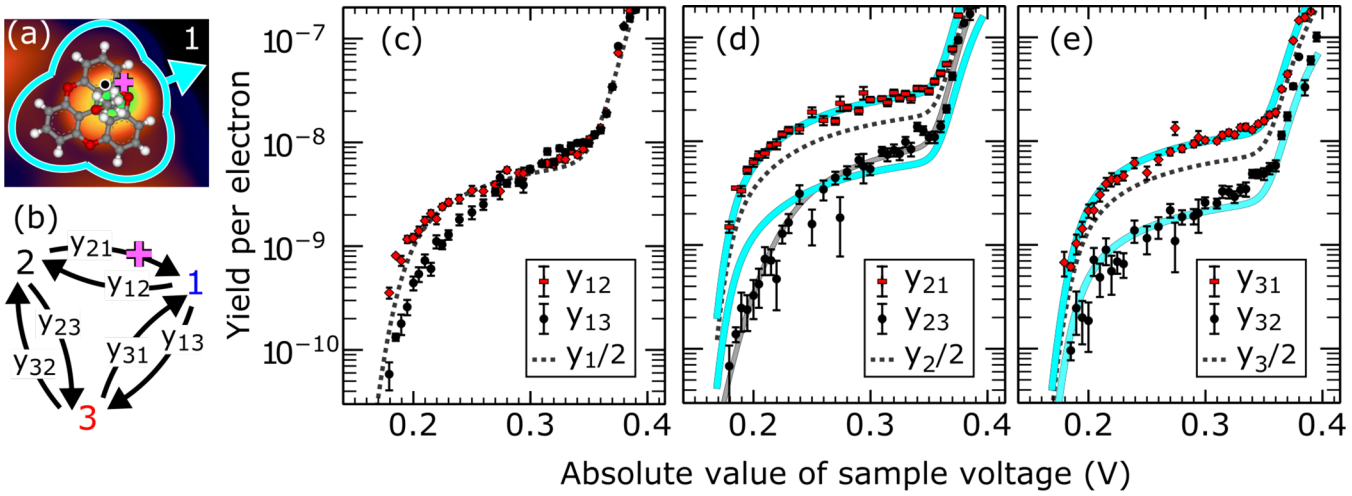

Figure 5. (a) STM topograph of ethoxy-TOTA with a calculated scaled molecular structure overlaid. The magenta cross (black dot) indicates the same positions as the white cross (circle) in Figure 1c−e. Both positions allow distinguishing states 1−3 (*cf.* Figure 1c−e) as distinct current levels at constant tip height. (b) Definition of the yields y_{ij} for switching from state *i* to state *j*. States 1, 2, and 3 are defined with respect to the tip position (magenta cross) during switching; that is, they correspond to the highest, middle, and lowest current level, respectively (*cf.* Figures 2 and 1c−e). (c, d) Measured yields y_{ij} for switching out of state (c) 1, (d) 2, and (e) 3 with the tip positioned at the magenta cross in (a). While the data points at high yield are based on 20 000 switching events, the lowest yield corresponds to 5 events. Bars indicate the standard deviation σ expected from a Poisson process. Dashed lines show fits to $y_i/2$ using eq S1 (SI, Section I) and correspond to the expected yields when switching is not directional. The upper (lower) solid turquoise lines in (d) and (e) represent the fits of $y_i/2$ (dashed lines) multiplied with a factor of 1.65 (0.35). Direct fits to y_{ij} (not shown) and y_i indicate active vibrational modes at 176 to 184 meV and 373 to 400 meV. The fits to y_{13} (not shown) and y_{23} [solid gray line in (d)] suggest vibrational modes at ∼206 and 231 meV, respectively.

weakens the hydrogen bonds between the moiety and the platform and in turn efficiently decays into a rotation. In other words, the combination of the energy barrier, the vibrational energy gap, and the type of vibrational modes (Figures S2 and S3) are consistent with the absence of rotation of ethyl-TOTA ($Y < 10^{-12}$) at electron energies below ∼350 meV. The importance of C−H stretching modes has been reported for other electron-induced processes[50] such as on-surface rotation,[12,27,51] hopping,[52] and synthesis.[53]

Analogous to ethyl-TOTA, the second abrupt increase of the action spectrum of ethoxy-TOTA at ∼370 meV is caused by C−H stretching vibrational modes of the moiety. However, the first abrupt increase in the action spectrum is related to one or several C−H bending vibrational mode(s) of energy ∼180 meV located on the moiety (SI, Section II and left arrow in Figure 4).

The barrier for rotation is lower in ethoxy-TOTA (∼140 meV), where several vibrational modes below the onset of the gap (∼200 meV) are capable of decaying into rotation, and as a result, the situation is drastically different. The relevant vibrations are C−H bending modes and therefore directly affect the CH···O bonds that stabilize the orientation of the ethoxy group (Figure S2). The experimental action spectra (Figure 3) suggest that these pure ethoxy modes indeed efficiently induce the rotation, while all other modes below 350 meV do not. In line with this observation, the other calculated modes between 140 and 350 meV are mainly vibrations of the platform (cf. Figure 4b) and are therefore less likely to lead to ethoxy rotation.

The relevant vibrational modes and rotation energy barriers are illustrated in Figure 4c−f. Two series of modes with energies of ∼180 and ∼370 meV, common for the two moieties, may effectively decay into a rotation. For ethyl-TOTA, the calculated rotational energy barrier is 195 mV (purple curve in Figure 4e). The vibrational modes at 180 meV therefore cannot provide enough energy for the rotation of the moiety (Figure 4e), and only the subsequent relevant vibrational modes at 370 mV may induce a rotation (Figure 4f). In contrast, for ethoxy-TOTA, the energy barrier (140 mV) is low enough such that both relevant series of modes can, in principle, transmit sufficient energy for the rotation (Figure 4c,d). This explains the presence of two abrupt increases in the yield of ethoxy-TOTA (Figure 3).

The energies of the C−H stretching modes are approximately twice as high as those of the C−H bending modes of the ethoxy group (*cf.* right and left arrows in Figure 3). Time-resolved measurements with picosecond light pulses on liquid hydrocarbons showed a highly efficient decay of C−H stretching modes into two C−H bending modes.[54] We speculate that an efficient *simultaneous* excitation of two C−H bending modes *via* the decay of a C−H stretching mode causes drastically higher (by more than 3 orders) switching yield of ethoxy-TOTA compared to ethyl-TOTA ($|V| > 350$ meV, Figure 3). This scenario is supported by the fact that an excitation of a single C−H bending mode of the ethoxy moiety is ∼10 times more efficient in inducing rotation than a single C−H stretching mode of the ethyl moiety.

In principle, tunneling electrons could also sequentially excite two vibrational modes (vibrational ladder climbing) without a preceding excitation of a high-energy mode. However, such a multielectron process would lead to a switching rate proportional to I^N where $N > 1$, in contrast to $N = 1$ experimentally observed (not shown).

Separate calculations of ethyl-TOTA on Au(111) (not shown) reveal an additional piece of important information. The energy barriers for moiety rotation and the vibrational modes of interest ($\hbar\omega > 130$ meV) hardly change upon adsorption, indicating that the TOTA platform efficiently

https://dx.doi.org/10.1021/acsnano.0c00029
ACS Nano 2020, 14, 3907−3916

decouples the functional moieties from the substrate as intended. Important gas-phase properties of a molecule are preserved.

Microscopic Yields and Directionality of the Rotation Steps. Next, we experimentally studied microscopic switching events of the three-state rotors, *i.e.*, switching from an initial state i to a final state j. The microscopic yields y_{ij} (Figure 5b) were obtained from time series of I at various sample voltages (SI, Section III). The total yield Y is linked to y_{ij} as follows:

$$Y = \sum_i \left(\alpha_i \sum_{j \neq i} y_{ij} \right) \tag{2}$$

where α_i is the probability of finding the rotor in an initial state i. To verify the consistency of all microscopic yields presented below, we derived the stationary solutions of the three-state master equation with y_{ij} as input (SI, Section III). Less than 4% variation is observed between the α_i estimated from the measurements and the α_i resulting from the master equation.

First, data from ethoxy-TOTA (Figure 1a and c–e, with two OH-TOTA neighbors close to ethoxy-TOTA) are discussed. The STM tip was positioned at a location (magenta cross in Figure 5a) equivalent to that indicated by a white cross in Figure 1c–e. This tip position makes the states **1**–**3** inequivalent, which allows obtaining three distinct current values (feedback off) in time series. y_{31} and y_{32} (Figure 5e, red and black symbols, respectively) are voltage dependent as expected from the overall yield (Figure 3). For $V \lesssim 330$ mV, y_{31} is 5 times larger than y_{32}. In other words, switching out of state **3** is directional.

For further analysis, we first fitted the sum $y_3 = y_{31} + y_{32}$, *i.e.*, switching events starting in state **3**, using eq S1 (SI Section I). Assuming nondirectional switching, we obtain the dotted line in Figure 5e with vibrational modes at ∼180 and ∼375 meV, in agreement with the energies ∼180 and ∼365 meV extracted from the action spectra (Figure 3). The obtained fit is scaled by 1.65/2 and 0.35/2 (turquoise lines in Figure 5d) to match y_{31} and y_{32}, respectively. These factors are related to the probability p_{ij} of switching from state i to j where

$$p_{ij} = \frac{y_{ij}}{\sum_{j \neq i} y_{ij}} \tag{3}$$

$p_{31} = 1.65/2 \approx 0.83$ ($p_{32} = 1 - p_{31} \approx 0.17$) for $|V| \lesssim 360$ mV. A reduction by 10–20% occurs when the second vibrational mode at ∼370 meV may be excited. The difference between p_{31} and p_{32} is related to the directionality of the rotation and strongly depends on the tip position (SI, Section IV). The directionality is mostly induced by the tip and the result of an attractive interaction between the tip and the moiety. Indeed, we observed that the favored final state is the one closest to the tip position (Figure 5 and SI, Section IV). For example, state **1** is preferred as a final state over **2** when the tip is located as indicated in Figure 5a and b (magenta cross).

Consequently, switching from state **2** (Figure 5d) also preferably ends in state **1** with $p_{21} \approx 0.83$. y_{21} is higher than any other microscopic yield of ethoxy-TOTA and actually exceeds the total yield Y. Note that there is no contradiction in having some of the microscopic yields larger than the total yield because the former ones are weighed by the probability of finding the initial state (<1) to give the total yield (eq 2). $y_2/2$ is fitted using eq S1 and scaled by 1.65 and 0.35 to obtain the lower and higher turquoise lines in Figure 5d,e. Clear deviations from the experimental y_{23} data are observed, especially for $|V| < 250$ mV, and suggest that the directionality depends on the sample voltage. Indeed, p_{21} evolves from ∼95% for $V \approx 180$ mV to ∼80% for $V \approx 250$ mV. Because $y_{23} = y_2 - y_{12}$, the yield y_{21} has similar deviations to y_{23} but of opposite sign. While the variations of y_{23} from the non-voltage-dependent directionality case (turquoise line in Figure 5d) are significant, they represent only a small fraction of y_{21} and are therefore barely observable in Figure 5d. We speculate that they are due to small tip-height changes with the voltage, which in turn mainly affects y_{21}. Indeed, the ethoxy moiety passes below the tip for switching from state **2** to **1**.

Finally, we consider switching from state **1** (Figure 5c). For $|V| \gtrsim 270$ mV, we hardly observe any directionality. Given that the STM tip is positioned close to the symmetry plane of state **1** (cross in Figure 1c), the final states **2** and **3** are almost equivalent and similar yields y_{12} and y_{13} are expected. However, there are deviations between y_{12} and y_{13} with a clear preference of **2** as final state for $V < 270$ mV. Similar to the yields in Figure 5d, these deviations may be linked to the tip that is located above the path of rotation, *i.e.*, between configurations **1** and **2**.

Tuning the Directionality of the Rotation. The ethoxy moiety seems to be attracted by the tip, which leads to a directionality of the rotation. The adsorption geometry of the molecule relative to the substrate atoms and neighboring molecules may also influence the energetic landscape of the ethoxy moiety and, in turn, affect the directionality. In the following, we discuss the influence of (i) the tip position, (ii) the adsorption geometry, and (iii) neighboring molecules on the directionality.

Additional microscopic yield data (SI, Section IV) were recorded, where the tip has been laterally displaced by 0.15 nm (dot in Figures 5a and 1c–e). As expected, the total yield Y is hardly affected by the change of tip position. However, the microscopic yields y_{ij} are drastically modified and reflect the different symmetry of the tip–molecule system. The new tip position is close to the symmetry plane of state **3**, leaving states **1** and **2** approximately equivalent. In turn, the switching from the initial state **3** shows fairly low directionality ($p_{31} \lesssim 0.6$, $p_{32} \gtrsim 0.4$). Moreover, the switching between **1** and **2** occurs with almost identical yields, $y_{12} \approx y_{21}$, in contrast to $y_{21} \approx 5\ y_{12}$ observed with the previous tip position. Therefore, a displacement of the tip as small as 0.15 nm can have a drastic effect on the directionality. For the new position, the favored final state **1** is the one closest to the tip, which is consistent with an attractive force between the ethoxy moiety and the tip.

An important role of the substrate appears to be rather unlikely because the platform decouples the moiety from the surface. Nevertheless, the adsorption geometry of ethoxy-TOTA on Au(111) is chiral, as inferred from DFT calculations along with STM data.[38,49] It breaks the symmetry of the substrate and induces a chirality of the molecule–substrate system, while the molecule itself is hardly changed upon adsorption, *i.e.*, remains achiral. Indeed, the mirror plane of the molecule is rotated by ∼−4° (enantiomer left) or by ∼+4° (enantiomer right) relative to a close-packed ⟨110⟩ direction of Au(111). We measured microscopic yields as the ones shown in Figure 5 on two different enantiomers but did not observe a significant variation of the directionality. Therefore, within the uncertainty of the measurements, the directionality is not affected by the substrate.

https://dx.doi.org/10.1021/acsnano.0c00029
ACS Nano 2020, 14, 3907–3916

As to factor (iii), adjacent TOTA molecules without substitution at the central carbon atom were observed to strongly affect the directionality of switching, whereas neighboring OH-TOTA and ethoxy-TOTA molecules were passive. In particular, when the tip is positioned above ethoxy-TOTA close to an adjacent bare TOTA molecule (Figure 6a),

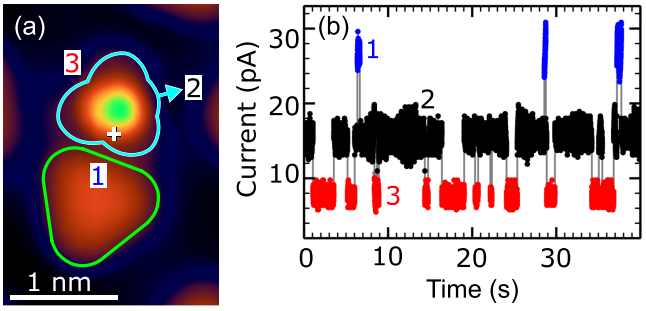

Figure 6. (a) STM topograph showing a single ethoxy molecule (turquoise) adjacent to a bare TOTA platform (light green). The image was processed by merging the raw data with a smoothed and inverted Laplace-filtered image. Tunnel parameters: 100 mV, 30 pA. (b) Time series of the tunneling current measured with the tip positioned over the cross in (a). V = 300 mV was applied, and the current feedback was opened at I = 7 pA. The current levels 1−3 correspond to states 1−3 (*cf.* Figure 1c−e). The states are indicated in (a), where the orientation of the ethoxy moiety corresponds to state 2.

the switching into state **1**, *i.e.*, rotation of the moiety toward the adjacent TOTA, is efficiently suppressed. At 300 mV, y_{21} and y_{31} are respectively reduced by factors of ∼10 and ∼5 compared to the case without neighboring TOTA molecules. Most switching events instead occur between states **2** and **3** (Figure 6b). We attribute this striking effect to Coulomb repulsion between the moiety and the TOTA neighbor. Indeed, adsorbed TOTA molecules are positively charged, as evidenced by the fact that TOTA in contrast to ethoxy- and ethyl-TOTA molecules do not form clusters on Au(111).[49] The topmost ethyl moiety of ethoxy-TOTA is most probably also positively charged because of the bond with electronegative oxygen. The measurements show that the electrostatic repulsion exceeds the attraction to state **1** caused by the STM tip.

States **2** and **3** are almost symmetric with respect to the adjacent bare platform. Switching between these states is therefore expected to be mainly controlled by the tip position. Indeed, switching from state **3** to state **2**, where the moiety is closer to the tip, is more efficient than the reverse process. The corresponding directionality induced by the tip ($y_{32} \approx 5y_{23}$) is similar to the case without a TOTA neighbor (Figure 5d,e where $y_{21} \approx 4.7y_{23}$ and $y_{31} \approx 4.7y_{32}$). The net result of the various yields is that the molecule with a neighbor prefers state **2** (Figure 6b) instead of state **1**, which exhibits the largest lifetime when no TOTA is present (Figure 2). Modifications of residence times and reaction yields by adsorbates have also been reported for other systems, such as intramolecular hydrogen transfer in a porphycene molecule on Cu(110) and phthalocyanine molecules on Ag(111).[55,56]

We did not observe a significant influence of OH-TOTA or ethoxy-TOTA neighbors on the directionality of switching. This may be expected because OH-TOTA or ethoxy-TOTA molecules do not repel each other on Au(111), which indicates that they are significantly less charged than TOTA.[49] In these cases, the tip position determines the directionality.

We also investigated the microscopic yields of the ethyl moiety in ethyl-TOTA (data not shown). The topmost methyl moiety tends to switch into the state that minimizes the separation from the tip. The measured directionalities are rather low ($p_{21,31}$ = 60−70%), similar to those of ethoxy-TOTA at large voltages, $|V| > 350$ mV. The reduced directionality is possibly related to the excitation of the C−H stretching vibrational mode that occurs in this energy range in ethyl-TOTA and ethoxy-TOTA.

We then employed the tip-induced control of the directionality to perform clockwise or anticlockwise rotation of an ethoxy moiety (Figure 7). At least two different tip

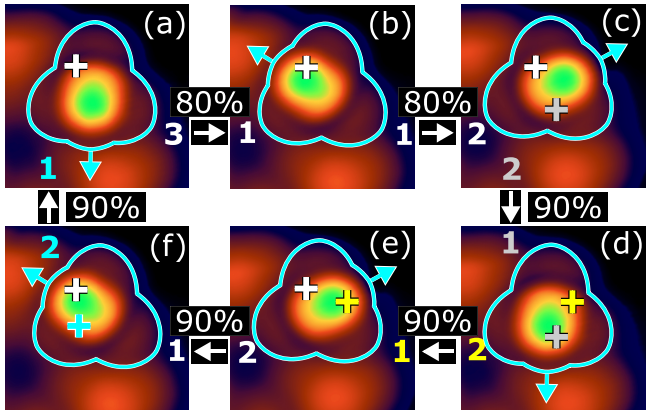

Figure 7. (a−f) STM topographs of the same ethoxy-TOTA molecule (marked with a turquoise border). From (a) to (d) the torsion angle θ_{oxy} was switched at 185 mV in a clockwise direction and from (d) to (f) and back to (a) in an anticlockwise direction. Two crosses in (c)−(f) indicate the tip positions used for switching into and from the state. For example, in (c) the gray and white crosses indicate the tip positions for current injection between topographs (b) to (c) and between (c) and (d). As the labeling of the states depends on the tip position, the color of the labels (numbers) indicates which tip position is used as a reference.

positions are necessary to obtain a complete rotation (*e.g.*, white and gray crosses in Figure 7a−d). The tip-induced directionality allows realizing a complete rotation without backward steps with a success rate of $\sim 0.90^3 = 0.73$.

CONCLUSIONS

We present a model study of two closely related molecular stepper motors that were designed to work on a metal substrate under excitation with tunneling electrons in an STM. The motors are composed of the TOTA platform as a stator and ethoxy and ethyl moieties as rotors. The platform approach reduces the complex interactions with the metal and thus preserves important properties built into the gas-phase molecules. This simplifies a detailed analysis and also defines three symmetry equivalent positions where the rotor is stabilized *via* CH···O bonds. Current-induced rotation of the moieties is demonstrated, the STM tip is used to generate directionality of the motion, modification of the directionality by adjacent charged adsorbates is revealed, and microscopic reaction yields are determined. By means of DFT calculations for the two related molecules, we show how the energies and displacement patterns of the vibrational modes, along with the

https://dx.doi.org/10.1021/acsnano.0c00029
ACS Nano 2020, 14, 3907−3916

barriers toward rotation, can lead to several orders of magnitude variation of the reaction yield.

METHODS

Synthesis of the Molecules. Functional groups were attached to the cationic TOTA platform by polar C−C and C−O bond formation. The synthesis of 12c-ethyl-4,8,12-trioxatriangulen (ethyl-TOTA) and OH-TOTA is described in refs 49 and 35, respectively.

The synthesis of 12c-ethoxy-4,8,12-trioxatriangulene (ethoxy-TOTA) was performed as follows: 390 mg (16.7 mmol) of sodium was added to 100 mL of ice-cooled ethanol and stirred for 1 h. Afterward 100 mg (269 μmol) of 4,8,12-trioxatrianguleniumtetrafluoroborate was added to the solution. After 20 min of ultrasonic treatment the mixture was stirred at room temperature for 17 h. The solution was concentrated to 20 mL, dissolved in 300 mL of anhydrous diethyl ether, and washed three times with 200 mL of ultrapure water. The combined aqueous layers were extracted with 200 mL of anhydrous diethyl ether. The combined organic layers were dried over magnesium sulfate and evaporated under reduced pressure. The beige solid was purified by sublimation at 1.2×10^{-2} mbar and 170 °C, yielding white crystals.

Yield: 42.0 mg (127 μmol, 47%). ^{1}H NMR (600 MHz, acetone-d_6, 300 K, TMS): δ = 7.51 (t, ^3J = 8.3 Hz, 3 H, *H*-2,6,10), 7.13 (d, ^3J = 8.3 Hz, 6 H, *H*-1,3,5,7,9,11), 3.04 (q, ^3J = 7.0 Hz, C-H_2), 0.82 (t, ^3J = 7.0 Hz, 3 H, C-H_3) ppm. ^{13}C NMR (151 MHz, acetone-d_6, 300 K, TMS): δ = 153.8 (*C*-3a, 4a, 7a, 8a, 11a, 12a), 131.1 (*C*-2, 6, 10), 112.0 (*C*-1, 3, 5, 7, 9, 11), 109.7 (*C*-7b, 11b, 12b), 57.4 (CH_3), 55.6 (*C*-12c), 15.4 (*C*-H_2) ppm. MS (EI, 70 eV): *m*/*z* (%) = 285.05(100) $[C_{19}H_9O_3]^+$, 330.09 (0.5) $[M]^+$. MS (EI, 70 eV): *m*/*z* (%) ($C_{21}H_{14}O_4$) measured 330.08915; calculated 330.08921. EA ($C_{21}H_{14}O_4$): measured C: 75.83, H: 4.00, N: 0.00%; calculated C: 76.36, H: 4.27, N: 0.00%. Melting point: 235.3 °C. FT-IR: $\tilde{\mu}$ = 2976.35 (w), 2324.29 (w), 2014.61 (w), 1615.44 (s), 1486.14 (s), 1456.42 (s), 1386.93 (w), 1341.62 (w), 1308.22 (w), 1260.34 (s), 1199.69 (m), 1159.52 (w), 1116.12 (w), 1067.35 (s), 1053.98 (m), 1013.23 (s), 957.27 (m), 943.30 (s), 902.46 (m), 882.00 (m), 785.23 (s), 774.61 (s), 759.51 (s), 737.88 (s), 664.74 (w) cm^{-1}.

Experimental Details. Measurements were performed with an STM operated at 4.6 K and in ultrahigh vacuum (base pressure 10^{-9} Pa). Au(111) surfaces and chemically etched W tips were cleaned by repeated Ar^+ bombardment and annealing. Submonolayers of ethyl-TOTA and the mixture of ethoxy-TOTA and OH-TOTA were sublimated onto flat Au(111) held at ambient temperature (<10^{-7} Pa and ~70 °C). After mounting into the STM, the tips were repeatedly indented into molecule-free areas of the substrate. To obtain a sharp tip, the sample was repeatedly contacted with the tip until the contacts were stable at a conductance $G \approx G_0$ and adatoms were imaged as circular protrusions of <700 pm diameter. All STM images were acquired using the constant-current mode.

Theoretical Details. The electronic structure and harmonic vibrational modes of free-standing ethoxy-TOTA and ethyl-TOTA were computed from Kohn−Sham DFT as implemented in VASP.[57] A plane-wave basis energy cutoff of 500 eV was used together with the optB88-vdW exchange−correlation functional.[58] Forces were relaxed to within 0.02 eV/Å, and vibrations were obtained with a finite-difference amplitude of 0.02 Å. The rotation barriers were computed using the nudged elastic band method[59] with a single intermediate image between the stable configurations.

ASSOCIATED CONTENT

Supporting Information

The Supporting Information is available free of charge at https://pubs.acs.org/doi/10.1021/acsnano.0c00029.

Action spectroscopy, mode analysis, master equation of rates and yields of a three-state rotor, and additional microscopic yields (PDF)

AUTHOR INFORMATION

Corresponding Authors

Torben Jasper-Toennies − *Institut für Experimentelle und Angewandte Physik, Christian-Albrechts-Universität, 24098 Kiel, Germany*; Email: jasper-toennies@physik.uni-kiel.de

Manuel Gruber − *Institut für Experimentelle und Angewandte Physik, Christian-Albrechts-Universität, 24098 Kiel, Germany*; orcid.org/0000-0002-8353-4651; Email: gruber@physik.uni-kiel.de

Authors

Sven Johannsen − *Institut für Experimentelle und Angewandte Physik, Christian-Albrechts-Universität, 24098 Kiel, Germany*

Thomas Frederiksen − *Donostia International Physics Center, E-20018 Donostia-San Sebastián, Spain; IKERBASQUE, Basque Foundation for Science, E-48013 Bilbao, Spain*; orcid.org/0000-0001-7523-7641

Aran Garcia-Lekue − *Donostia International Physics Center, E-20018 Donostia-San Sebastián, Spain; IKERBASQUE, Basque Foundation for Science, E-48013 Bilbao, Spain*; orcid.org/0000-0001-5556-0898

Torben Jäkel − *Otto-Diels-Institut für Organische Chemie, Christian-Albrechts-Universität, 24098 Kiel, Germany*

Fynn Roehricht − *Otto-Diels-Institut für Organische Chemie, Christian-Albrechts-Universität, 24098 Kiel, Germany*

Rainer Herges − *Otto-Diels-Institut für Organische Chemie, Christian-Albrechts-Universität, 24098 Kiel, Germany*; orcid.org/0000-0002-6396-6991

Richard Berndt − *Institut für Experimentelle und Angewandte Physik, Christian-Albrechts-Universität, 24098 Kiel, Germany*; orcid.org/0000-0003-1165-9065

Complete contact information is available at: https://pubs.acs.org/10.1021/acsnano.0c00029

Notes

The authors declare no competing financial interest.

ACKNOWLEDGMENTS

We thank the Deutsche Forschungsgemeinschaft (SFB 677 and SPP 1928-II (COORNETs)), the Spanish MINECO (Grant Nos. MAT2016-78293-C6-4-R and FIS2017-83780-P), and Diputación Foral de Gipuzkoa RED 2019-096 for financial support.

REFERENCES

(1) Schliwa, M.; Woehlke, G. Molecular Motors. *Nature* **2003**, *422*, 759−765.

(2) Kinbara, K.; Aida, T. Toward Intelligent Molecular Machines: Directed Motions of Biological and Artificial Molecules and Assemblies. *Chem. Rev.* **2005**, *105*, 1377−1400.

(3) Kassem, S.; van Leeuwen, T.; Lubbe, A. S.; Wilson, M. R.; Feringa, B. L.; Leigh, D. A. Artificial Molecular Motors. *Chem. Soc. Rev.* **2017**, *46*, 2592−2621.

(4) Lensen, D.; Elemans, J. A. A. W. Artificial Molecular Rotors and Motors on Surfaces: STM Reveals and Triggers. *Soft Matter* **2012**, *8*, 9053.

(5) Ni, C.; Wang, J.-Z. STM Sudies on Molecular Rotors and Motors. *Surf. Rev. Lett.* **2018**, *25*, 1841004.

(6) Gimzewski, J. K.; Joachim, C.; Schlittler, R. R.; Langlais, V.; Tang, H. Rotation of a Single Molecule within a Supramolecular Bearing. *Science* **1998**, *281*, 531−533.

(7) Stipe, B. C.; Rezaei, M. A.; Ho, W. Inducing and Viewing the Rotational Motion of a Single Molecule. *Science* **1998**, *279*, 1907−1909.

(8) Baber, A. E.; Tierney, H. L.; Sykes, E. C. H. A Quantitative Single-Molecule Study of Thioether Molecular Rotors. *ACS Nano* **2008**, *2*, 2385−2391.
(9) Gao, L.; Liu, Q.; Zhang, Y. Y.; Jiang, N.; Zhang, H. G.; Cheng, Z. H.; Qiu, W. F.; Du, S. X.; Liu, Y. Q.; Hofer, W. A.; Gao, H.-J. Constructing an Array of Anchored Single-Molecule Rotors on Gold Surfaces. *Phys. Rev. Lett.* **2008**, *101*, 197209.
(10) Manzano, C.; Soe, W.-H.; Wong, H. S.; Ample, F.; Gourdon, A.; Chandrasekhar, N.; Joachim, C. Step-by-Step Rotation of a Molecule-Gear Mounted on an Atomic-Scale Axis. *Nat. Mater.* **2009**, *8*, 576−579.
(11) Zhong, D.; Blömker, T.; Wedeking, K.; Chi, L.; Erker, G.; Fuchs, H. Surface-Mounted Molecular Rotors with Variable Functional Groups and Rotation Radii. *Nano Lett.* **2009**, *9*, 4387−4391.
(12) Tierney, H. L.; Murphy, C. J.; Jewell, A. D.; Baber, A. E.; Iski, E. V.; Khodaverdian, H. Y.; McGuire, A. F.; Klebanov, N.; Sykes, E. C. H. Experimental Demonstration of a Single-Molecule Electric Motor. *Nat. Nanotechnol.* **2011**, *6*, 625−629.
(13) Tierney, H. L.; Murphy, C. J.; Sykes, E. C. H. Regular Scanning Tunneling Microscope Tips Can Be Intrinsically Chiral. *Phys. Rev. Lett.* **2011**, *106*, 010801.
(14) Palma, C.-A.; Björk, J.; Rao, F.; Kühne, D.; Klappenberger, F.; Barth, J. V. Topological Dynamics in Supramolecular Rotors. *Nano Lett.* **2014**, *14*, 4461−4468.
(15) Ohmann, R.; Meyer, J.; Nickel, A.; Echeverria, J.; Grisolia, M.; Joachim, C.; Moresco, F.; Cuniberti, G. Supramolecular Rotor and Translator at Work: On-Surface Movement of Single Atoms. *ACS Nano* **2015**, *9*, 8394−8400.
(16) Krönlein, A.; Kügel, J.; Kokh, K. A.; Tereshchenko, O. E.; Bode, M. Energetic and Spatial Mapping of Resonant Electronic Excitations. *J. Phys. Chem. C* **2016**, *120*, 13843−13849.
(17) Sun, K.; Luo, J.-Y.; Zhang, X.; Wu, Z.-J.; Wang, Y.; Yuan, H.-K.; Xiong, Z.-H.; Li, S.-C.; Xue, Q.-K.; Wang, J.-Z. Supramolecular Motors on Graphite Surface Stabilized by Charge States and Hydrogen Bonds. *ACS Nano* **2017**, *11*, 10236−10242.
(18) Gehrig, J. C.; Penedo, M.; Parschau, M.; Schwenk, J.; Marioni, M. A.; Hudson, E. W.; Hug, H. J. Surface Single-Molecule Dynamics Controlled by Entropy at Low Temperatures. *Nat. Commun.* **2017**, *8*, 14404.
(19) Eisenhut, F.; Meyer, J.; Krüger, J.; Ohmann, R.; Cuniberti, G.; Moresco, F. Inducing the Controlled Rotation of Single o-MeO-DMBI Molecules Anchored on Au(111). *Surf. Sci.* **2018**, *678*, 177−182.
(20) Lu, H.-L.; Cao, Y.; Qi, J.; Bakker, A.; Strassert, C. A.; Lin, X.; Ernst, K.-H.; Du, S.; Fuchs, H.; Gao, H.-J. Modification of the Potential Landscape of Molecular Rotors on Au(111) by the Presence of an STM Tip. *Nano Lett.* **2018**, *18*, 4704−4709.
(21) Simpson, G. J.; García-López, V.; Boese, A. D.; Tour, J. M.; Grill, L. How to Control Single-Molecule Rotation. *Nat. Commun.* **2019**, *10*, 4631.
(22) Wang, W.; Shi, X.; Jin, M.; Minot, C.; Hove, M. A. V.; Collin, J.-P.; Lin, N. Electron Stimulation of Internal Torsion of a Surface-Mounted Molecular Rotor. *ACS Nano* **2010**, *4*, 4929−4935.
(23) Perera, U. G. E.; Ample, F.; Kersell, H.; Zhang, Y.; Vives, G.; Echeverria, J.; Grisolia, M.; Rapenne, G.; Joachim, C.; Hla, S.-W. Controlled Clockwise and Anticlockwise Rotational Switching of a Molecular Motor. *Nat. Nanotechnol.* **2013**, *8*, 46−51.
(24) Zhang, Y.; Kersell, H.; Stefak, R.; Echeverria, J.; Iancu, V.; Perera, U. G. E.; Li, Y.; Deshpande, A.; Braun, K.-F.; Joachim, C.; Rapenne, G.; Hla, S.-W. Simultaneous and Coordinated Rotational Switching of All Molecular Rotors in a Network. *Nat. Nanotechnol.* **2016**, *11*, 706−712.
(25) Homberg, J.; Lindner, M.; Gerhard, L.; Edelmann, K.; Frauhammer, T.; Nahas, Y.; Valášek, M.; Mayor, M.; Wulfhekel, W. Six State Molecular Revolver Mounted on a Rigid Platform. *Nanoscale* **2019**, *11*, 9015−9022.
(26) Zhang, Y.; Calupitan, J. P.; Rojas, T.; Tumbleson, R.; Erbland, G.; Kammerer, C.; Ajayi, T. M.; Wang, S.; Curtiss, L. A.; Ngo, A. T.; Ulloa, S. E.; Rapenne, G.; Hla, S. W. A Chiral Molecular Propeller Designed for Unidirectional Rotations on a Surface. *Nat. Commun.* **2019**, *10*, 3742.
(27) Stipe, B. C.; Rezaei, M. A.; Ho, W. Coupling of Vibrational Excitation to the Rotational Motion of a Single Adsorbed Molecule. *Phys. Rev. Lett.* **1998**, *81*, 1263−1266.
(28) Pan, S.; Fu, Q.; Huang, T.; Zhao, A.; Wang, B.; Luo, Y.; Yang, J.; Hou, J. Design and Control of Electron Transport Properties of Single Molecules. *Proc. Natl. Acad. Sci. U. S. A.* **2009**, *106*, 15259−15263.
(29) Wasio, N. A.; Slough, D. P.; Smith, Z. C.; Ivimey, C. J.; Thomas, S. W., III; Lin, Y.-S.; Sykes, E. C. H. Correlated Rotational Switching in Two-Dimensional Self-Assembled Molecular Rotor Arrays. *Nat. Commun.* **2017**, *8*, 16057.
(30) Balema, T. A.; Ulumuddin, N.; Murphy, C. J.; Slough, D. P.; Smith, Z. C.; Hannagan, R. T.; Wasio, N. A.; Larson, A. M.; Patel, D. A.; Groden, K.; McEwen, J.-S.; Lin, Y.-S.; Sykes, E. C. H. Controlling Molecular Switching *via* Chemical Functionality: Ethyl *vs* Methoxy Rotors. *J. Phys. Chem. C* **2019**, *123*, 23738−23746.
(31) Rusch, T. R.; Schlimm, A.; Krekiehn, N. R.; Flöser, B. M.; Röhricht, F.; Hammerich, M.; Lautenschläger, I.; Strunskus, T.; Herges, R.; Tuczek, F.; Magnussen, O. M. Ordered Adlayers of a Combined Lateral Switch and Rotor. *J. Phys. Chem. C* **2019**, *123*, 13720−13730.
(32) Ernst, K.-H. Molecular Chirality at Surfaces. *Phys. Status Solidi B* **2012**, *249*, 2057−2088.
(33) Mishra, P.; Hill, J. P.; Vijayaraghavan, S.; Rossom, W. V.; Yoshizawa, S.; Grisolia, M.; Echeverria, J.; Ono, T.; Ariga, K.; Nakayama, T.; Joachim, C.; Uchihashi, T. Current-Driven Supramolecular Motor with *In Situ* Surface Chiral Directionality Switching. *Nano Lett.* **2015**, *15*, 4793−4798.
(34) Larson, A. M.; Groden, K.; Hannagan, R. T.; McEwen, J.-S.; Sykes, E. C. H. Understanding Enantioselective Interactions by Pulling Apart Molecular Rotor Complexes. *ACS Nano* **2019**, *13*, 5939−5946.
(35) Martin, J. C.; Smith, R. G. Factors Influencing the Basicities of Triarylcarbinols. The Synthesis of Sesquixanthydrol. *J. Am. Chem. Soc.* **1964**, *86*, 2252−2256.
(36) Baisch, B.; Raffa, D.; Jung, U.; Magnussen, O. M.; Nicolas, C.; Lacour, J.; Kubitschke, J.; Herges, R. Mounting Freestanding Molecular Functions onto Surfaces: The Platform Approach. *J. Am. Chem. Soc.* **2009**, *131*, 442−443.
(37) Jasper-Tönnies, T.; Garcia-Lekue, A.; Frederiksen, T.; Ulrich, S.; Herges, R.; Berndt, R. Conductance of a Freestanding Conjugated Molecular Wire. *Phys. Rev. Lett.* **2017**, *119*, 066801.
(38) Jasper-Tönnies, T.; Garcia-Lekue, A.; Frederiksen, T.; Ulrich, S.; Herges, R.; Berndt, R. High-Conductance Contacts to Functionalized Molecular Platforms Physisorbed on Au(1 1 1). *J. Phys.: Condens. Matter* **2019**, *31*, 18LT01.
(39) Valášek, M.; Mayor, M. Spatial and Lateral Control of Functionality by Rigid Molecular Platforms. *Chem. - Eur. J.* **2017**, *23*, 13538−13548.
(40) Jung, U.; Schütt, C.; Filinova, O.; Kubitschke, J.; Herges, R.; Magnussen, O. Photoswitching of Azobenzene-Functionalized Molecular Platforms on Au Surfaces. *J. Phys. Chem. C* **2012**, *116*, 25943−25948.
(41) Koumura, N.; Zijlstra, R. W. J.; van Delden, R. A.; Harada, N.; Feringa, B. L. Light-Driven Monodirectional Molecular Rotor. *Nature* **1999**, *401*, 152−155.
(42) Carroll, G. T.; Pollard, M. M.; van Delden, R.; Feringa, B. L. Controlled Rotary Motion of Light-Driven Molecular Motors Assembled on a Gold Film. *Chem. Sci.* **2010**, *1*, 97.
(43) Motobayashi, K.; Kim, Y.; Ueba, H.; Kawai, M. Insight into Action Spectroscopy for Single Molecule Motion and Reactions through Inelastic Electron Tunneling. *Phys. Rev. Lett.* **2010**, *105*, 076101.
(44) Frederiksen, T.; Paulsson, M.; Ueba, H. Theory of Action Spectroscopy for Single-Molecule Reactions Induced by Vibrational Excitations with STM. *Phys. Rev. B: Condens. Matter Mater. Phys.* **2014**, *89*, 035427.

https://dx.doi.org/10.1021/acsnano.0c00029
ACS Nano 2020, 14, 3907−3916

(45) Kim, Y.; Motobayashi, K.; Frederiksen, T.; Ueba, H.; Kawai, M. Action Spectroscopy for Single-Molecule Reactions − Experiments and Theory. *Prog. Surf. Sci.* **2015**, *90*, 85−143.
(46) Persson, B. N. J.; Baratoff, A. Inelastic Electron Tunneling from a Metal Tip: The Contribution from Resonant Processes. *Phys. Rev. Lett.* **1987**, *59*, 339−342.
(47) Lorente, N.; Persson, M. Theory of Single Molecule Vibrational Spectroscopy and Microscopy. *Phys. Rev. Lett.* **2000**, *85*, 2997−3000.
(48) Monturet, S.; Lorente, N. Inelastic Effects in Electron Transport Studied with Wave Packet Propagation. *Phys. Rev. B: Condens. Matter Mater. Phys.* **2008**, *78*, 035445.
(49) Jasper-Tönnies, T.; Poltavsky, I.; Ulrich, S.; Moje, T.; Tkatchenko, A.; Herges, R.; Berndt, R. Stability of Functionalized Platform Molecules on Au(111). *J. Chem. Phys.* **2018**, *149*, 244705.
(50) Arnolds, H. Vibrational Dynamics of Adsorbates − *Quo Vadis*? *Prog. Surf. Sci.* **2011**, *86*, 1−40.
(51) Shchadilova, Y. E.; Tikhodeev, S. G.; Paulsson, M.; Ueba, H. Rotation of a Single Acetylene Molecule on Cu(001) by Tunneling Electrons in STM. *Phys. Rev. Lett.* **2013**, *111*, 186102.
(52) Kim, H. W.; Han, M.; Shin, H.-J.; Lim, S.; Oh, Y.; Tamada, K.; Hara, M.; Kim, Y.; Kawai, M.; Kuk, Y. Control of Molecular Rotors by Selection of Anchoring Sites. *Phys. Rev. Lett.* **2011**, *106*, 146101.
(53) Kim, Y.; Komeda, T.; Kawai, M. Single-Molecule Reaction and Characterization by Vibrational Excitation. *Phys. Rev. Lett.* **2002**, *89*, 126104.
(54) Laubereau, A.; Kaiser, W. Vibrational Dynamics of Liquids and Solids Investigated by Picosecond Light Pulses. *Rev. Mod. Phys.* **1978**, *50*, 607−665.
(55) Kumagai, T.; Hanke, F.; Gawinkowski, S.; Sharp, J.; Kotsis, K.; Waluk, J.; Persson, M.; Grill, L. Controlling Intramolecular Hydrogen Transfer in a Porphycene Molecule with Single Atoms or Molecules Located Nearby. *Nat. Chem.* **2014**, *6*, 41−46.
(56) Kügel, J.; Klein, L.; Leisegang, M.; Bode, M. Analyzing and Tuning the Energetic Landscape of H_2Pc Tautomerization. *J. Phys. Chem. C* **2017**, *121*, 28204−28210.
(57) Kresse, G.; Furthmüller, J. Efficient Iterative Schemes for *Ab Initio* Total-Energy Calculations Using a Plane-Wave Basis Set. *Phys. Rev. B: Condens. Matter Mater. Phys.* **1996**, *54*, 11169−11186.
(58) Klimes, J.; Bowler, D. R.; Michaelides, A. Chemical Accuracy for the van der Waals Density Functional. *J. Phys.: Condens. Matter* **2010**, *22*, 022201.
(59) Mills, G.; Jónsson, H.; Schenter, G. K. Reversible Work Transition State Theory: Application to Dissociative Adsorption of Hydrogen. *Surf. Sci.* **1995**, *324*, 305−337.

https://dx.doi.org/10.1021/acsnano.0c00029
ACS Nano 2020, 14, 3907−3916

Supporting Information: Rotation of Ethoxy and Ethyl Moieties on a Molecular Platform on Au(111)

Torben Jasper-Toennies,[*,†] Manuel Gruber,[*,†] Sven Johannsen,[†] Thomas Frederiksen,[‡,¶] Aran Garcia-Lekue,[‡,¶] Torben Jäkel,[§] Fynn Roehricht,[§] Rainer Herges,[§] and Richard Berndt[†]

†*Institut für Experimentelle und Angewandte Physik, Christian-Albrechts-Universität, 24098 Kiel, Germany*

‡*Donostia International Physics Center, DIPC, Paseo Manuel de Lardizabal 4, E-20018 Donostia-San Sebastián, Spain*

¶*IKERBASQUE, Basque Foundation for Science, E-48013 Bilbao, Spain*

§*Otto-Diels-Institut für Organische Chemie, Christian-Albrechts-Universität, 24098 Kiel, Germany*

E-mail: jasper-toennies@physik.uni-kiel.de; gruber@physik.uni-kiel.de

1 Action Spectroscopy

1.1 Fit Function

The action spectra in the manuscript have been fitted using:[S1]

$$Y(V) = \sum_{\Omega} Y_{\Omega}(V), \tag{S1}$$

where the sum is over the vibrational modes of energy $\hbar\Omega$ ($\hbar$: reduced Planck constant) involved in the rotation. In the present cases of ethoxy-TOTA and ethyl-TOTA these are only two modes and one, respectively. For a given vibrational mode with energy $\hbar\Omega$, the reaction yield Y_{Ω}, *i.e.*, the probability to induce a rotation per electron, reads:[S1]

$$Y_{\Omega}(V) = K(\Omega)\left[1 + \frac{|eV| - \hbar\Omega}{|eV|}E_G(|eV| - \hbar\Omega) - \frac{|eV| + \hbar\Omega}{|eV|}E_G(|eV| + \hbar\Omega) + \frac{\rho_v(|eV|)\sigma_G^2}{|eV|}\right], \tag{S2}$$

$$E_G(X) = \frac{1}{2}\frac{\mathrm{Erf}(X/\sqrt{2}\sigma_G)}{\mathrm{Erf}(\Omega/\sqrt{2}\sigma_G)}, \tag{S3}$$

where $K(\Omega)$ is a dimensionless prefactor, $\mathrm{Erf}(X)$ the error function, V the applied sample voltage and e the elementary charge. Equation S2 assumes Gaussians with a standard deviation σ_G centered at $\pm\hbar\Omega$ for the vibrational density of states (vDOS) of the relevant modes:

$$\rho_v(\omega) = \frac{1}{\sigma_G\sqrt{2\pi}}\frac{1}{\mathrm{Erf}(\Omega/\sqrt{2}\sigma)}\left\{\exp\left(-\frac{(\hbar\omega - \hbar\Omega)^2}{2\sigma_G^2}\right) - \exp\left(-\frac{(\hbar\omega + \hbar\Omega)^2}{2\sigma_G^2}\right)\right\}, \tag{S4}$$

which takes into account all broadening effects encountered in practice like, *e. g.*, thermal, noise/instrumental and intrinsic lifetime broadening.[S2]

Equation S2 depends on three parameters: Ω, $K(\Omega)$ and σ_G. Therefore, fitting experi-

mental action spectra requires three fit parameters per vibrational mode.

1.2 Interpretation and Simplification of the Fit Function

The width σ_G of the vibrational modes is typically on the order of 10 meV in our experiments. The last term in Equation S2 can be neglected for $|eV| > \hbar\Omega + 3\,\sigma_G$ because $\rho_\nu(eV)\,\sigma_G$ converges to zero (less than 1.2 % deviation). Moreover, $E_G(|eV| - \hbar\Omega)$ and $E_G(|eV| + \hbar\Omega)$ effectively converge to 1/2 (less than 0.5 % deviation). Equation S2 simplifies to:

$$Y_\Omega(V) = \; K(\Omega)\,\frac{|eV| - \hbar\Omega}{|eV|}\,\theta(|eV| - \hbar\Omega), \tag{S5}$$

where θ is the step function, which allows to extend the definition of Equation S5 to voltages $|eV| < \hbar\omega$. Equation S5 corresponds to the reaction yield due to single vibrational mode with a vDOS described by a Dirac δ-function.[S2] Related expressions have been used to describe the inelastic excitations in solid-state tunneling junctions.[S3]

We would like to emphasize that the derivation of Equation S2 is done in the wide-band limit, where the densities of states of the tip and adsorbate+surface are assumed to be independent of the energy. Under these conditions, the factor $(|eV| - \hbar\Omega)/|eV|$ gives the proportion of tunneling electrons whose energy is sufficient to excite the vibrational mode of energy $\hbar\Omega$. The prefactor $K(\Omega)$ describes the combined probability of (i) a tunneling electron with sufficient energy to excite the vibrational mode of interest and (ii) the mode to decay into the reaction of interest, *e.g.*, a rotation.

Figure S1 illustrates that Equation S5 is a very good approximation of the yield, except close to the excitation energy. The deviation between the yields given by Equations S2 and S5 becomes more pronounced when the broadening of the vibrational mode σ_G is increased. However, the relative difference decays rapidly and is on the order of 1 % for sample voltages $|eV| - \hbar\Omega > 2\sigma_G$ (Fig. S1b). This rapid decay also occurs when Lorentzians ρ_L are assumed for the vibrational DOS (cf. Equation S4). Considering that yields for $|eV| < \hbar\Omega + 2\sigma_G$ are

usually low and may be barely experimentally measurable within a resonable time, Equation S5 is generally well suited to fit experimental action spectra for $|eV| - \hbar\Omega > 2\sigma_G$. It neglects broadening effects and reduces the fit parameters to the energy of the vibrational mode $\hbar\Omega$ and the prefactor.

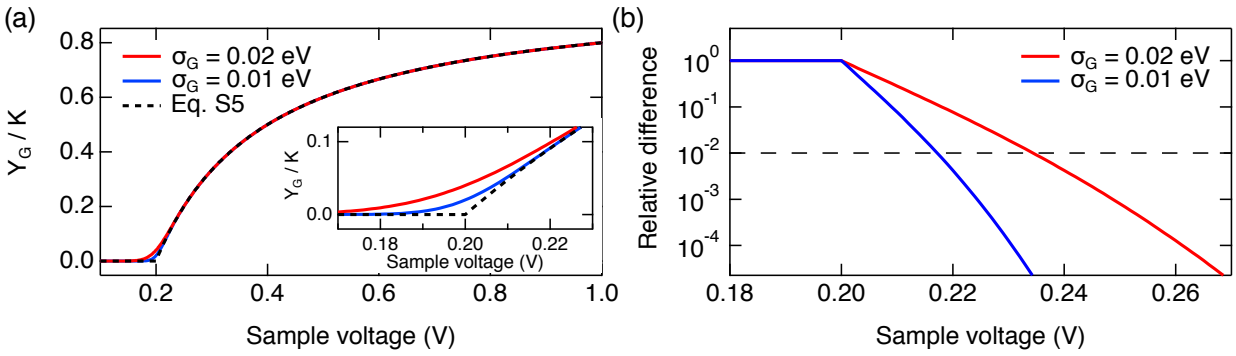

Figure S1: (a) Yields inferred from Equation S2 for a vibrational mode at $\hbar\Omega = 0.2$ eV with a gaussian broadening $\sigma_G = 0.02$ eV (red) and $\sigma_G = 0.01$ eV (blue). The dashed black curve corresponds to the yield given by the simplified Equation S5. The inset is a zoom for sample voltages close to the excitation energy of the vibrational mode. (b) Relative difference between the yields given by Equations S2 and S5.

1.3 Discussion of the Prefactor K

The probability of an electron with sufficient energy to induce vibrational excitation depends on the electron-phonon coupling. This probability can be on the order of 1 to 10 %.[S4–S6] Although K is the combined probability of (i) excitation of a given vibrational mode and (ii) decay of this mode into the reaction of interest, we will see that K is effectively independent of the electron-phonon coupling.

The reaction yield may be rewritten as:[S2]

$$Y_\Omega(V) = \tilde{K}(\Omega)\ \frac{I_{in}(V,\Omega)}{I(V)}, \tag{S6}$$

where $\tilde{K}(\Omega)$ is a prefactor describing the efficiency of the excited mode with energy $\hbar\Omega$ in inducing the reaction. $I_{in}(V,\Omega)/I(V)$ is the related inelastic proportion of the tunneling current, *i. e.* the fraction of tunneling electrons exciting the vibrational mode $\hbar\Omega$. It may be

worth mentioning that a larger electron-phonon coupling increases the ratio $I_{in}(V,\Omega)/I(V)$. The prefactor $\tilde{K}(\Omega)$ is actually included in the factor $K(\Omega)$ in Equations S2 and S5.

For an over-barrier process, *i.e.*, when enough energy is transferred to the system to overcome the reaction barrier (in contrast to tunneling processes), the prefactor is determined by:[S2]

$$\tilde{K}(\Omega) \cong \frac{\gamma_{RC}(\Omega)}{\gamma_{eh}(\Omega)}, \tag{S7}$$

where $\gamma_{RC}(\Omega)$ is the conversion rate of the vibrational mode $\hbar\Omega$ into decay channels that induce the reaction and $\gamma_{eh}(\Omega)$ is the rate at which the vibrational mode decays into other channels. The predominant decay channel very often is electron-hole pair creation,[S2] which is also related to the electron-phonon coupling. Therefore, while a large electron-phonon coupling leads to a larger proportion of electrons exciting the vibrational mode of energy $\hbar\Omega$, it effectively does not affect the yield because γ_{eh} increases in the same proportion (cf. Equations S6 and S7).

Following the derivations in Ref. S2,

$$K(\Omega) = \frac{\gamma_{eh}(\Omega)\,\tilde{K}(\Omega)}{2\Omega\rho_a(E_F)\,\Gamma} \cong \frac{\gamma_{RC}(\Omega)}{2\Omega\rho_a(E_F)\,\Gamma}, \tag{S8}$$

where $\rho_a(E_F)$ is the DOS of the adsorbate at the Fermi energy E_F and Γ is the width of the electronic resonance. Thus, K depends on the conversion rate γ_{RC} of the vibrational mode into the reaction and on the system parameters $\rho_a(E_F)$ and Γ.

In the off-resonant tunneling regime, relevant for the ethoxy-TOTA and ethyl-TOTA molecules, the position of the current-carrying orbital E_a with respect to E_F satisfies the relation $|E_a - E_F| \gg \Gamma/2$, and one has $\rho_a(E_F) \approx \Gamma/(2\pi(E_a - E_F)^2)$. Consequently, the prefactor can be expressed as:

$$K(\Omega) \approx \pi\frac{\gamma_{RC}(\Omega)}{\Omega}\frac{(E_a - E_F)^2}{\Gamma^2}. \tag{S9}$$

As may be expected, K, and hence the reaction yield Y, is proportional to the conversion rate γ_{RC} relative to the oscillation frequency Ω as well as to the orbital level position $|E_a - E_F|$ relative to the resonance width Γ.

From the analysis of the prefactor $K(\Omega)$, we predict that reaction yields on (partially) insulating surfaces should be significantly larger than on metal surfaces because Γ would be significantly reduced. Alternatively, the electronic decoupling may be implemented in the molecules themselves. In that respect, for the same functional unit (*e.g.*, rotor), larger yields are expected for physiborbed systems than for chemisorbed systems.

2 Mode Analysis

Figures S2 and S3 illustrate some of the calculated vibrational modes of the moiety for ethoxy- and ethyl-TOTA. The length of the green arrows is associated to the displacement amplitude of the corresponding atoms.

We recall that the rotors have three stable positions, where two hydrogen atoms of the moieties bind via a CH···O hydrogen bond to one of the three oxygen atoms of the platform. Vibrational modes of the moiety involving a large displacement of the corresponding hydrogen atoms may lead to an effective weakening of the hydrogen bond. In turn, such a vibrational mode may efficiently decay into a rotation of the moiety.

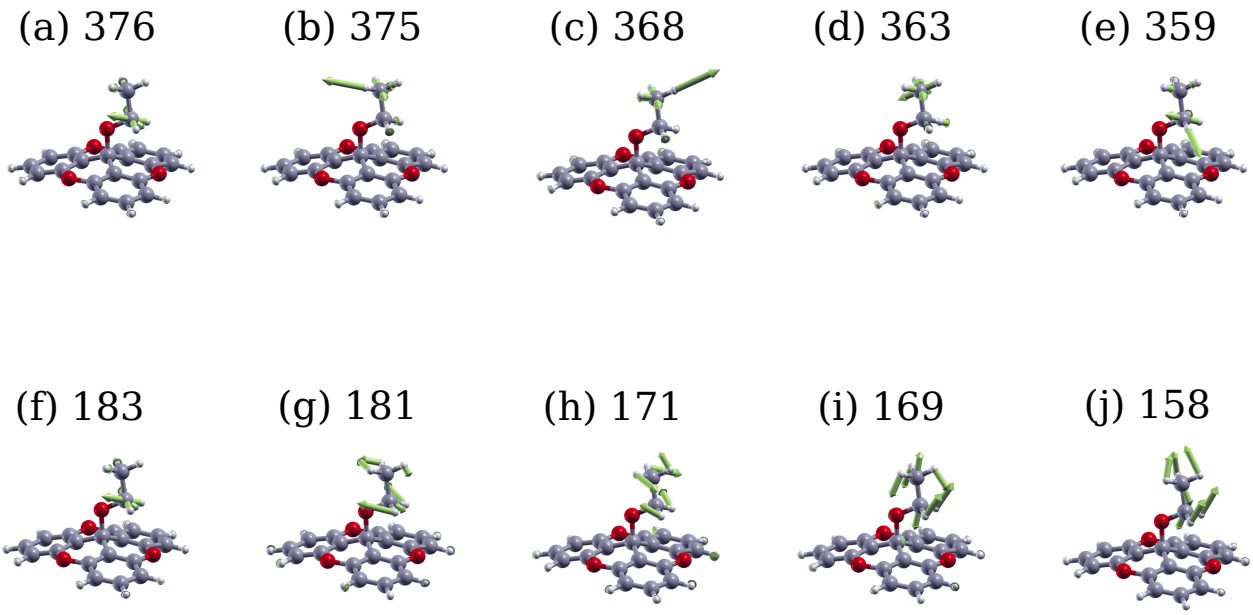

Figure S2: Calculated vibrational modes that are predominantly localized on the moeity of ethoxy-TOTA. Mode energies are given in meV. (a–e) C–H stretching modes. (f–j) C–H bending modes.

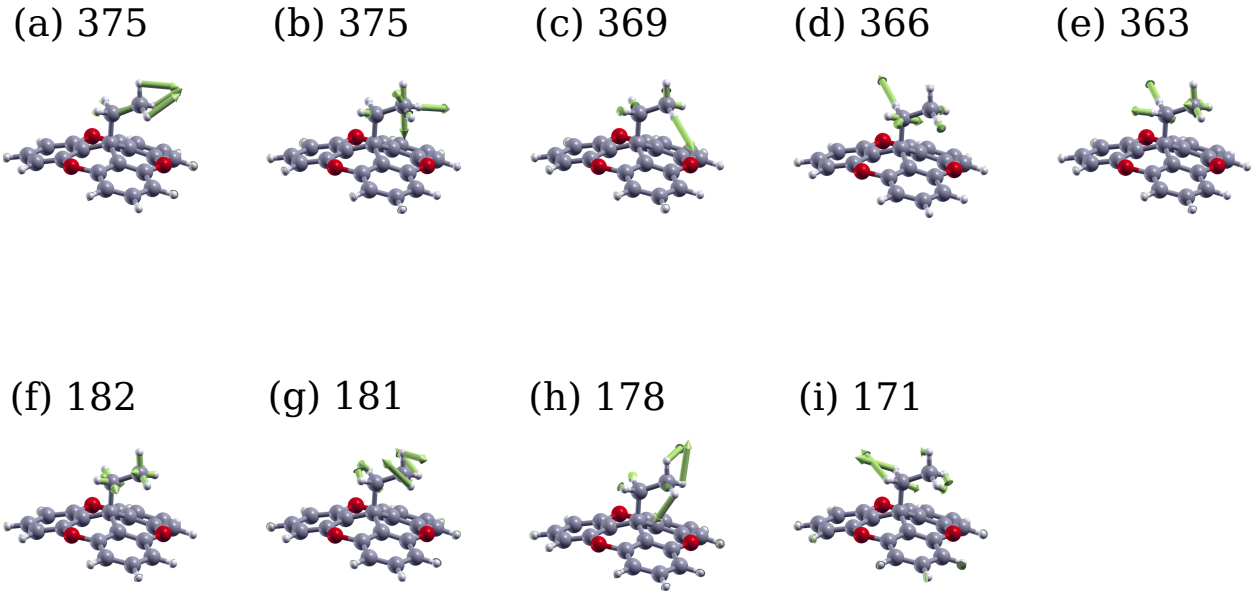

Figure S3: Calculated vibrational modes that are predominantly localized on the moeity of ethyl-TOTA. Mode energies are given in meV. (a–e) C–H stretching modes. (f–i) C–H bending modes.

3 Master Equation of Rates and Yields of a Three-State Rotor

A master equation connects the probability p_i of finding the system in the state i at the time t with the microscopic rates r_{ij} for switching from an initial state i to a final state j:

$$\frac{dp_i}{dt} = \sum_{i \neq j} p_j r_{ji} - p_i r_{ij}. \tag{S10}$$

The three-state rotors studied in the manuscript are switched via single tunneling electrons. Changing the tunneling current affects the switching rates r_{ij} and the probabilities p_i, and therefore Equation S10 depends on the tunneling current. To circumvent this limitation, the master equation with respect to time (Equation S10) is rewritten to a master equation with respect to the number of tunneling electrons n as a (quasi) continuous parameter. Note that representing n as a continuous parameter is justified by the low yield of the investigated rotor, where one out of every 10^6 electrons may induce a switching event. The transformation is achieved via the following substitutions:

$$t \implies n \tag{S11}$$

$$p_i \implies \alpha_i \tag{S12}$$

$$r_{ij} \implies y_{ij}, \tag{S13}$$

where α_i is the probability to find state i after n tunneling electrons and y_{ij} is the number of switching events per tunneling electron ($y_{ij} < 1$). Note that y_{ij} is effectively a yield, but in contrast to the total yield Y (Equation S6), it considers a particular transition from state i to state j. With these substitutions the master equation reads:

$$\frac{d\vec{\alpha}}{dn} = \begin{pmatrix} -(y_{12}+y_{13}) & y_{21} & y_{31} \\ y_{12} & -(y_{21}+y_{23}) & y_{32} \\ y_{13} & y_{23} & -(y_{31}+y_{32}) \end{pmatrix} \vec{\alpha}\ , \quad \vec{\alpha} := \begin{pmatrix} \alpha_1 \\ \alpha_2 \\ \alpha_3 \end{pmatrix} \tag{S14}$$

Its stationary solution ($\frac{d\vec{\alpha}}{dn} = 0$) is

$$\begin{pmatrix} \alpha_1 \\ \alpha_2 \\ \alpha_3 \end{pmatrix} = \begin{pmatrix} \frac{y_{23}\,y_{31} + y_{32}\,y_{21} + y_{21}\,y_{31}}{y_{12}\,y_{23} + y_{23}\,y_{31} + y_{31}\,y_{12} + y_{32}\,y_{21} + y_{13}\,y_{32} + y_{21}\,y_{13} + y_{12}\,y_{32} + y_{23}\,y_{13} + y_{31}\,y_{21}} \\ \frac{y_{32} + (y_{12} - y_{32})\alpha_1}{y_{21} + y_{23} + y_{32}} \\ 1 - \alpha_1 - \alpha_2 \end{pmatrix}. \tag{S15}$$

Experimentally, time-series of the tunneling current have been acquired (Figure 2 of the manuscript) at a given voltage and a given tip-sample distance. α_i and y_{ij} are determined experimentally using:

$$\alpha_i = \frac{n_i}{\sum_{i=1}^{3} n_i} = \frac{t_i I_i/e}{\sum_{i=1}^{3} t_i I_i/e}, \tag{S16}$$

$$y_{ij} = \frac{N_{ij}}{n_i}, \tag{S17}$$

where I_i is the current corresponding to state i, t_i (n_i) the time (number of tunneling electrons) during which the system is in the state i, and N_{ij} the number of observed transitions from state i to state j. The consistency of the microscopic yields y_{ij} was verified by inserting them into Equation S15 and comparing the resulting α_i with those obtained experimentally. The corresponding deviations are systematically below 4 %, which shows that the uncertainties on the experimentally determined microscopic yields are rather limited.

4 Additional Microscopic Yields of Ethoxy-TOTA

In contrast to the total yields, the microscopic yields y_{ij} of ethoxy-TOTA drastically depend on the precise tip position. Lateral displacements of the tip as small as 0.15 nm can significantly change the microscopic yields. For instance, for the data shown in Figures 5c–d of the manuscript, the tip was positioned above the white cross displayed in Figure S4. Changing the location of the tip to the black dot (Figure S4) leads to drastically different microscopic yields as shown in Figure S4c–d. For example, the microscopic yield y_{12} (y_{13}) is higher (lower) by approximately a factor 5 when the tip is above the black dot compared to the case when the tip is above the white cross.

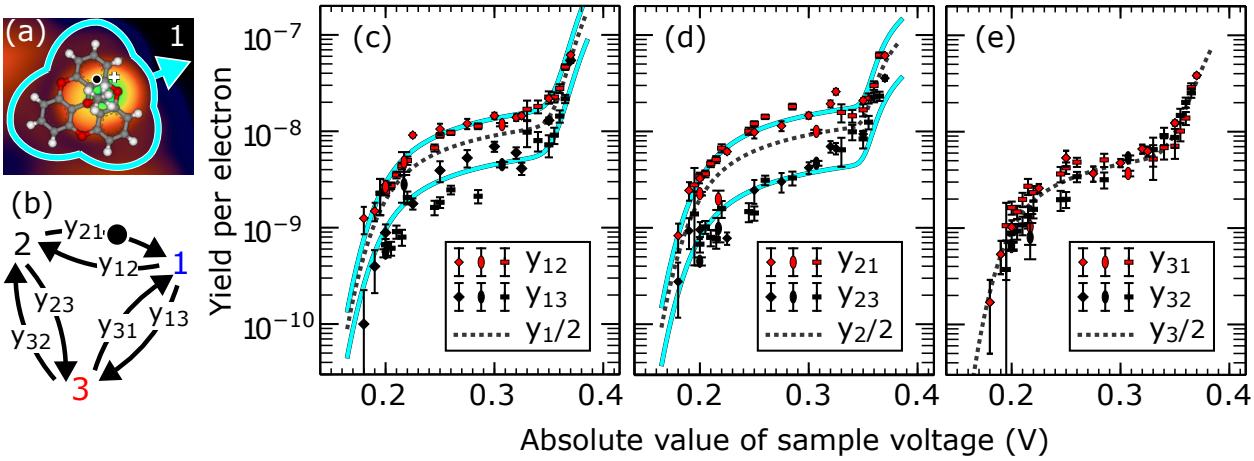

Figure S4: (a) STM topograph of ethoxy-TOTA with an overlayed scaled molecular structure. The black dot (white cross) indicates the same relative positions as the white circle (cross) in Figures 1(c–e). Both positions allow to distinguish states **1**-**3** [cf. Figs. 1(c–e)] as distinct current levels at constant tip height. (b) Definition of the yields y_{ij} for switching from state $\boldsymbol{i}$ to state $\boldsymbol{j}$. States **1**, **2**, and **3** are defined with respect of the tip position (black dot) during switching, *i. e.* they correspond to the highest, middle, and lowest current level, respectively. (c–d) Measured yields y_{ij} for switching out of state (c) **1**, (d) **2** and (e) **3** with the tip positioned over the black dot in (a). Different symbols correspond to different STM tips and molecules. While the data points at high yields are based on ≈ 500 switching events, the lowest yield corresponds to ≈ 2 events. Bars indicate the standard deviation σ expected for a Poisson process. Dashed lines correspond to fits to $y_i/2$ using Equation S2, and show the expected yields of non-directional switching. The fits indicate electron-induced vibrational modes between 177 to 185 meV and 355 to 400 meV. The upper (lower) solid turquoise lines in (c) and (d) represent the fits of $y_i/2$ (dashed lines) multiplied by a factor of 1.5 (0.5) and 1.6 (0.4), respectively.

The modifications of y_{ij} actually reflect the changed symmetry of the tip-molecule system. While the white cross (Figure S4a) is close to the symmetry plane of state **1**, the black dot is closer to the symmetry plane passing through state **3**. Therefore, for the tip position depicted by the black dot (white cross), the states **1** and **2** (**2** and **3**) are approximately equivalent. Indeed, the directionality for switching out of state **3** is relatively low for the tip position marked with a black dot ($p_{31} \lesssim 0.6$, $p_{32} \gtrsim 0.4$, Fig. S4e), in contrast to the data obtained at the tip position marked with a white cross (Figure 5e). Switching out of state **1** is directional for the tip position marked with a black dot with $y_{12} \approx 3 \times y_{13}$ for $|V| < 350$ mV (red and black symbols in Fig. S4c), whereas no directionality is observed at the white cross for $|V| \gtrsim 270$ meV (red and black symbols in Fig. 5c). Finally, switching from state **2** is directional with both tip positions. It may be worth mentioning that only two levels instead of three are observed when the tip is positioned in a symmetry plane.

At the tip position marked with a black dot, state **1** still corresponds to the smallest distance between the ethoxy moiety and the tip and therefore remains favored as a final state. This suggests that the STM tip induces directionality via an attractive force on the ethoxy moiety, as discussed in the manuscript.

References

(S1) Frederiksen, T.; Paulsson, M.; Ueba, H. Theory of Action Spectroscopy for Single-Molecule Reactions Induced by Vibrational Excitations with STM. *Phys. Rev. B* **2014**, *89*, 035427.

(S2) Kim, Y.; Motobayashi, K.; Frederiksen, T.; Ueba, H.; Kawai, M. Action Spectroscopy for Single-Molecule Reactions – Experiments and Theory. *Prog. Surf. Sci.* **2015**, *90*, 85–143.

(S3) Lambe, J.; McCarthy, S. L. Light Emission from Inelastic Electron Tunneling. *Phys. Rev. Lett.* **1976**, *37*, 923–925.

(S4) Persson, B. N. J.; Baratoff, A. Inelastic Electron Tunneling from a Metal Tip: The Contribution from Resonant Processes. *Phys. Rev. Lett.* **1987**, *59*, 339–342.

(S5) Lorente, N.; Persson, M. Theory of Single Molecule Vibrational Spectroscopy and Microscopy. *Phys. Rev. Lett.* **2000**, *85*, 2997–3000.

(S6) Monturet, S.; Lorente, N. Inelastic Effects in Electron Transport Studied with Wave Packet Propagation. *Phys. Rev. B* **2008**, *78*, 035445.